colloids and interfaces

MDPI

Article

Effect of Sodium Tripolyphosphate on the Grinding and Separation of Copper–Tin Polymetallic Sulfide Ore

Xiaobo Liu, Qingfei Xiao, Mengtao Wang, Chao Zheng, Yiqi Cui and Saizhen Jin *

Faculty of Land Resource Engineering, Kunming University of Science and Technology, Kunming 650093, China; 15714036588@163.com (X.L.)
* Correspondence: 20230042@kust.edu.cn

Abstract

The complex mineral composition and heterogeneous intergrowth characteristics of copper–tin polymetallic sulfide ores make it difficult to obtain an appropriate particle-size distribution and sufficient mineral liberation during grinding, which can affect subsequent separation. This study investigated the effects of sodium tripolyphosphate (STPP) as a grinding aid on a copper–tin polymetallic sulfide ore from the Datun Plant in Gejiu, Yunnan, China. Grinding and separation tests, together with mineralogical and surface characterization using MapsMin, SEM-EDS, zeta-potential and contact-angle measurements, and DLVO/EDLVO calculations, were conducted to evaluate the effects of STPP on grinding and subsequent separation. The grinding results showed that, compared with the lime-only condition (0.10 wt% lime), the addition of 0.025 wt% STPP increased the proportion of the target size fraction (−0.15 + 0.019 mm) by 1.76%, without a marked increase in the fine fraction (−0.019 mm) or the coarse fraction (+0.15 mm). Compared with the lime-only condition, the addition of 0.025 wt% STPP increased the grade and recovery of the copper flotation concentrate by 0.20% and 3.54%, respectively, and those of the cassiterite gravity concentrate by 0.44% and 14.31%, respectively. The overall Sn recovery of the combined gravity separation and flotation process increased from 92.58% under the lime-only condition to 93.56% with the addition of 0.025 wt% STPP, but decreased to 92.39% when the STPP dosage was increased to 0.050 wt%. Automated mineralogical analysis showed that STPP addition increased the complete liberation degrees of cassiterite and bornite, while varying degrees of improvement were also observed for other major minerals. With the addition of 0.025 wt% STPP, the maximum particle size decreased from 820.95 to 495.30 μm, and D90 decreased from 374 to 237 μm relative to the lime-only condition. Surface characterization and DLVO/EDLVO analysis indicated that STPP altered mineral surface properties and interparticle interactions, which may have contributed to the observed changes in particle-size distribution and mineral liberation.

Keywords: copper-tin polymetallic sulfide ore; sodium tripolyphosphate; flotation; gravity separation; contact angle; zeta potential; DLVO; MapsMin

Check for updates

Academic Editors: Tuan Nguyen, Zhiqiang Huang, Sheng Liu and Chen Cheng

Received: 25 August 2026
Revised: 28 October 2026
Accepted: 29 October 2026
Published: 2 November 2026

Copyright: © 2026 by the authors. Licensee MDPI, Basel, Switzerland. This article is an open access article distributed under the terms and conditions of the Creative Commons Attribution (CC BY) license.

1. Introduction

Grinding is the final stage of particle size reduction before mineral separation, and the characteristics of grinding products, such as particle size and mineral liberation, critically influence the efficiency of subsequent separation processes, such as flotation and gravity separation [1–3]. Although grinding is an effective method for reducing particle size, it remains one of the most energy-intensive operations in mineral processing because of its

high energy consumption and low energy efficiency. As a key stage in mineral beneficiation, comminution strongly influences the operating costs and energy consumption of mineral-processing operations. Comminution typically accounts for approximately 30–50% of total mining operating costs and represents a major share of the energy consumed in mineral processing [4,5]. Therefore, improving grinding efficiency and reducing energy consumption are essential for sustainable mineral processing. Two main approaches are commonly used to enhance grinding efficiency: optimizing grinding processes or equipment performance [6,7], and introducing chemical reagents into the comminution process, commonly referred to as grinding aids, to improve grinding performance [8,9].

Grinding aids are widely used in industries such as mineral processing, cement production, ceramics, and fertilizer manufacturing [10–14]. In mineral processing, grinding aids have mainly been applied to the grinding of single metallic or non-metallic ores. Mao et al. [15] reported that the combined use of triisopropanolamine (TIPA) and triethanolamine (TEA) during quartz grinding significantly enhanced grinding efficiency and flotation recovery by improving quartz hydrophobicity, collector adsorption, and particle dispersion. Fan et al. [9] found that SHMP enhances mica grinding efficiency by disrupting the crystalline structure, improving slurry dispersion through physical adsorption, and promoting surface roughening and crack formation. Wang et al. [16] demonstrated that pre-treatment with Z-164D solution significantly reduced the Bond work index and uniaxial compressive strength of bauxite by introducing structural defects through physicochemical adsorption and water–molecule interactions, thereby facilitating ore breakage. Chipakwe et al. [17] developed an environmentally friendly polysaccharide-based grinding aid (PGA) for magnetite grinding, which reduced energy consumption, narrowed particle size distribution, increased surface area, and improved flotation performance. Similarly, Xie et al. [10] showed that the combined use of NM-3 and ammonium acetate significantly enhanced hematite grinding efficiency by decreasing the proportions of both coarse and over-ground particles. These studies demonstrate that grinding aids can modify particle surface properties, improve slurry dispersion, and ultimately enhance grinding performance and mineral liberation.

Commonly used grinding aids in mineral processing include sodium tripolyphosphate (STPP) [12,18], sodium oxalate, acetone, potassium dihydrogen phosphate [18], Zalta™ GR20-587 (a commercial grinding aid; manufacturer: Solenis, Sweden), Zalta™ VM1122 (a commercial viscosity modifier; manufacturer: Solenis, Sweden), and sodium hydroxide [19]. Among these reagents, STPP is of interest because of its relatively low toxicity and high water solubility. However, the application of grinding aids in polymetallic ore grinding remains limited. Polymetallic ores typically contain complex mineral assemblages with distinct mechanical properties and surface characteristics, leading to differential responses of individual minerals to grinding aids. Consequently, a reagent that improves the grinding behavior of one mineral may not have the same effect on other minerals. Moreover, the liberation and recovery of multiple valuable minerals require appropriate control of particle-size distribution and mineral surface properties. Some grinding aids exhibit surface-active properties similar to those of flotation reagents [15,20], and their addition during grinding may alter mineral surface chemistry and affect subsequent flotation and gravity separation [21,22]. However, existing studies on STPP and other grinding aids have mainly focused on single minerals or relatively simple ore systems, with an emphasis on improving grinding performance. Their effects on particle dispersion, mineral liberation, and subsequent separation performance in complex polymetallic ores therefore remain insufficiently understood. In particular, the effects of STPP on particle-size distribution, fine-particle generation, and the liberation of valuable minerals with different surface prop-

erties, as well as the resulting changes in downstream separation performance, require further investigation.

Therefore, sodium tripolyphosphate (STPP) was selected as a grinding aid for a copper–tin polymetallic sulfide ore from the Datun Plant in Gejiu, China. The effects of STPP on grinding behavior, particle-size distribution, mineral liberation, and subsequent Cu and Sn separation performance were systematically investigated. Scanning electron microscopy (SEM) and energy-dispersive X-ray spectroscopy (SEM-EDS) were used to characterize mineral morphology and surface elemental composition, using a SU3900 scanning electron microscope (Hitachi High-Tech Corporation, Tokyo, Japan), while MapsMin automated mineralogical analysis was employed to evaluate mineral liberation characteristics. Zeta-potential and contact-angle measurements were conducted to characterize mineral surface properties. In addition, DLVO/EDLVO theoretical analysis was used to evaluate interparticle interactions and help interpret the possible effects of STPP addition on interactions involving cassiterite and copper sulfide minerals. This study provides an integrated assessment of STPP-assisted grinding and its implications for the separation of copper and tin from a complex polymetallic sulfide ore.

2. Materials and Methods

2.1. Materials

The polymetallic copper–tin sulfide ore used in the experiments was obtained from the Datun sulfide ore-processing plant, Gejiu, China. The raw ore was first crushed and screened using an XPS-Φ250 × 150 roller crushing and screening machine (Wuhan Prospecting Machinery Factory, Wuhai, China) to obtain two particle size fractions, −2 + 0.5 mm and −0.5 mm. The two size fractions were then blended at a mass ratio of 1:4 (−2 + 0.5 mm:−0.5 mm) to prepare the grinding feed. The elemental composition of the ore sample was determined by X-ray fluorescence (PANalytical B.V., Almelo, The Netherlands) analysis, and the results are presented in Table 1. The mineralogical composition of the ore sample was characterized using the MapsMin automated mineral analysis system, and the corresponding results are presented in Table 2. According to Table 2, the dominant minerals in the ore were calcite, pyrite, and pyrrhotite. The main copper-bearing minerals are bornite and covellite, whereas cassiterite is the primary tin-bearing mineral.

Table 1. Chemical composition of the ore sample determined by XRF analysis.

Elemental	F	Mg	Al	Si	S	K	Ca	Fe	Cu	Sn	Other
Content (%)	2.58	4.58	1.91	9.84	5.93	1.05	16.32	20.81	0.42	0.84	35.72

Table 2. Mineralogical composition of the ore sample determined by MapsMin automated mineral analysis.

Mineral Phase	Pyrite	Pyrrhotite	Siderite	Calcite	Dolomite	Quartz
Percent (%)	19.50	11.97	10.79	10.37	7.05	5.55
Mineral phase	**Biotite**	**Arsenopyrite**	**Hematite**	**Bornite**	**Cassiterite**	**Other**
Percent (%)	4.48	4.20	3.10	0.41	3.18	19.40

Pure cassiterite and bornite samples were purchased from Sichuan Province, China, and used for mineral surface characterization and interparticle interaction analysis. The cassiterite sample contained 95% SnO_2, while the bornite sample contained 61% Cu. Before use, the pure mineral samples were crushed, ground, and hand-sorted. Their mineralogical compositions were further characterized by X-ray diffraction (XRD), and the corresponding

diffraction patterns are presented in Figure 1. As shown in Figure 1, the main diffraction peaks of the samples were consistent with those of cassiterite and bornite, respectively, confirming that the samples were predominantly composed of cassiterite and bornite. The samples were therefore considered suitable for subsequent contact-angle, zeta-potential, and theoretical interaction analyses.

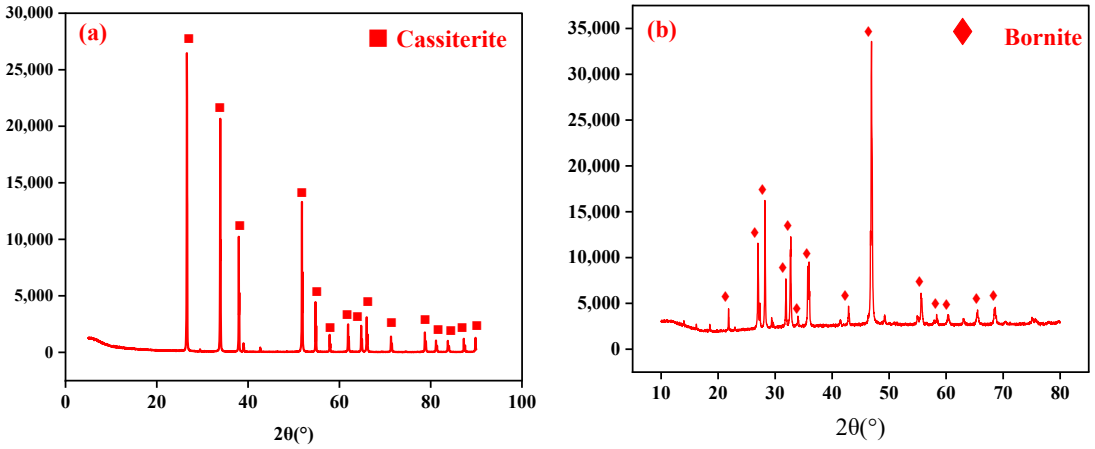


Figure 1. X-ray diffraction patterns of cassiterite (**a**) and bornite (**b**).

Analytical-grade sodium tripolyphosphate (STPP) was obtained from Tianjin Zhonglian Chemical Reagents Co., Ltd., Tianjin, China. Sodium hydroxide (NaOH), hydrochloric acid (HCl), copper sulfate ($CuSO_4$), lime (CaO), SN, P86, oxalic acid ($H_2C_2O_4$), and terpenic oil were of analytical grade and were obtained from the laboratory of Yunnan Tin Company, Kunming, China. In the grinding tests, lime was added at a fixed dosage of 0.10 wt%, whereas STPP was tested at dosages of 0.025–0.100 wt%. The other reagents were used in the flotation and separation tests according to the experimental conditions described below.

2.2. Methods

2.2.1. Grinding Tests

The grinding experiments were conducted using an XMQ 250 × 100 conical ball mill (Nanchang Liyuan Mining and Metallurgical Chaoyang Laboratory Equipment Manufacturing Co., Ltd., Nanchang, China), operating at a drum speed of 90 r/min. The effective volume of the mill was 6.65 L. The grinding media consisted of balls with diameters of 40, 30, and 20 mm, in a weight ratio of 4:4:2, with a media filling rate of 40%. Each test used 500 g of ore sample at a pulp concentration of 70%. The grinding time was determined based on the actual feed size requirements of the mineral flotation processing plant. According to preliminary grinding tests, the grinding time was set at 3 min 30 s. The ground products were first screened using sieves with openings of 0.15 and 0.074 mm. Subsequently, the particle size distribution of the −0.074 mm fraction was further determined using a laser particle size analyzer (BXF). The BXF analyzer provided cumulative particle size data at 0.045, 0.038, 0.028, and 0.019 mm. The particle size distribution was calculated based on the total grinding product by combining the sieve analysis and laser particle size analysis results, and the final results were reported as the average of three tests.

2.2.2. Copper and Tin Separation Tests

Based on the actual beneficiation flowsheet and reagent regime of the Datun beneficiation plant, this study investigated the effect of STPP addition during grinding on the subsequent beneficiation performance of copper and cassiterite from the polymetallic copper–tin sulfide ore. The ground products were successively subjected to copper flotation,

desulfurization flotation, cassiterite gravity separation using a shaking table, and cassiterite flotation, as illustrated in Figure 2. During grinding, lime (CaO) was fixed at 0.10 wt%, whereas STPP was added at 0, 0.025, and 0.05 wt%. After grinding, the entire pulp was transferred to a 1.5-L XFD single-cell flotation machine (Nanchang Liyuan Mining and Metallurgical Equipment Co., Ltd., Nanchang, China). The pulp pH was adjusted to 7.7 and maintained at this value using NaOH and HCl. The flotation machine was operated at an aeration rate of 0.15 m^3/h and a scraper speed of 20 r/min. Flotation times and reagent dosages were controlled according to the flowsheet in Figure 2. The desulfurization flotation product was subjected to gravity separation using an LYN(S)-1100 × 500 grooved-deck shaking table (Wuhan Prospecting Machinery Factory) at a feed pulp concentration of 20%, a stroke length of 10 mm, and a stroke frequency of 340 strokes min^{-1}. The resulting cassiterite product was further subjected to flotation. Except for the STPP dosage during grinding, all other reagent regimes and operating conditions were kept constant. All beneficiation tests were conducted in triplicate.

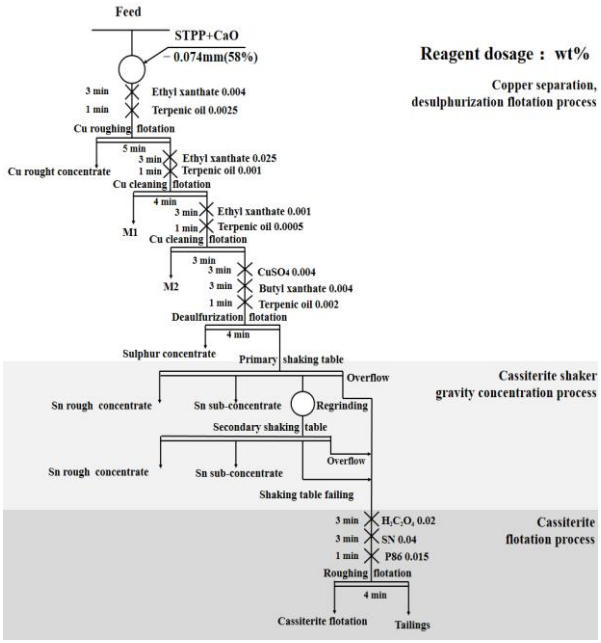


Figure 2. Flow chart of separation tests.

The recovery of the valuable components was calculated from the concentrate yield and the grades of the feed and concentrate according to Equation (1):

$$\varepsilon = \frac{\gamma\beta}{\alpha} \times 100\% \quad (1)$$

where ε is the recovery of the valuable component (%), γ is the concentrate yield (%), β is the grade of the valuable component in the concentrate (%), and α is the grade of the valuable component in the feed (%).

2.2.3. Mineral Liberation and Particle-Size Distribution Analysis

An automated mineralogy system (MapsMin, Thermo Fisher Scientific, Waltham, MA, USA) was employed to evaluate the mineral liberation and particle-size distribution of the ground polymetallic ore samples in the absence and presence of STPP. The system integrates a Thermo Scientific Apreo 2S scanning electron microscope (SEM) equipped with a Bruker XFlash 6|30 energy-dispersive X-ray spectroscopy (EDS) detector to acquire backscattered-

electron (BSE) images and elemental X-ray maps. Mineral phases were identified based on their compositional characteristics.

For sample preparation, the ore samples were ground for 3 min 30 s under two reagent conditions: 0.10 wt% lime alone and 0.10 wt% lime + 0.025 wt% STPP. The ground products were first classified into +0.074 mm and −0.074 mm fractions by sieving, followed by drying prior to automated mineralogical analysis. A total of 40,085 and 26,095 mineral particles were analyzed using MapsMin, respectively.

The samples were mixed with graphite at a mass ratio of 3:1 and embedded in epoxy resin. The mixture was thoroughly stirred and ultrasonicated to ensure uniform particle dispersion, followed by vacuum treatment to eliminate air bubbles before curing for 12 h. The cured samples were subsequently ground and polished until a scratch-free surface was achieved, as confirmed by optical microscopy. The polished sections were then carbon-coated to a thickness of approximately 6 nm using a LEICA EM ACE 200 (Leica Microsystems, Wetzlar, Germany). The prepared samples were analyzed using the Thermo Scientific Apreo 2S SEM (Thermo Fisher Scientific, Brno, Czech Republic). Mineral phase identification and particle characterization were performed using MapsMin, and the acquired EDS data were processed using NanoMin for mineralogical analysis. In the mineral liberation analysis, a mineral phase was considered liberated when its liberation degree was at least 90%. This criterion was applied consistently to all samples.

2.2.4. Scanning Electron Microscopy (SEM) and Energy-Dispersive X-Ray Spectroscopy (EDS) Analyses

The particle morphologies of the ore samples ground with 0.10 wt% CaO alone and with 0.10 wt% CaO plus 0.025 wt% STPP for 3 min 30 s were observed under vacuum using a scanning electron microscope (SU3900, Hitachi, Tokyo, Japan). A total of 0.2 g of sample was directly attached to conductive adhesive and sputter-coated with gold for 45 s using an Oxford Quorum SC7620 sputter coater operated at 10 mA. The sample morphology was then imaged using accelerating voltages of 5 and 15 kV [23].

2.2.5. Contact-Angle Measurements

The contact angles of pure mineral samples conditioned with different concentrations of STPP were measured using a JY-82B video contact-angle goniometer. The pre-polished mineral samples were conditioned in STPP solutions with concentrations of 0, 0.02, 0.04, 0.06, 0.08, and 0.10 wt% for 5 min. The pH of all STPP solutions was adjusted to 8.0 ± 0.2 using dilute NaOH or HCl solutions to maintain consistent experimental conditions. After conditioning, the mineral samples were removed and dried under ambient conditions. Deionized water was used as the probe liquid for contact-angle measurements. Three measurements were performed at different positions on each mineral surface, and the average value was reported.

2.2.6. Zeta Potential Measurements

The zeta potentials of pure mineral samples at different pH values and STPP dosages were measured using a Zetasizer Nano-ZS90 (Malvern Panalytical, Shanghai, China). All measurements were conducted at room temperature using 1×10^{-3} mol/L KCl as the background electrolyte.

Approximately 50 mg of mineral particles (<5 μm) were dispersed in 40 mL of electrolyte solution in a 100-mL beaker, with STPP dosages of 0 and 0.025 wt%. The pH of the suspensions was adjusted to the desired values using dilute NaOH or HCl solutions. The suspensions were magnetically stirred for 2 min to ensure adequate dispersion and then allowed to equilibrate for 5 min. A portion of each suspension was subsequently transferred

to a cuvette for zeta-potential measurement. Each experiment was performed three times, and the average value was used for analysis.

2.2.7. DLVO/EDLVO Theoretical Calculations

The DLVO theory was employed to evaluate the interparticle interactions and dispersion behavior of cassiterite and bornite particles. According to the classical DLVO theory, the total interaction energy between two particles is determined by the van der Waals and electrostatic double-layer interactions [24–28].

$$V_{\mathrm{DLVO}} = V_{\mathrm{vdW}} + V_{\mathrm{EDL}} \tag{2}$$

where V_{DLVO} is the total DLVO interaction energy, V_{vdW} is the van der Waals interaction energy, and V_{EDL} is the electrostatic double-layer interaction energy. Because classical DLVO theory does not account for non-DLVO interactions, such as hydrophobic, steric, and hydration interactions, an extended DLVO (EDLVO) model was used. In the present study, only the hydrophobic interaction was additionally considered; steric and hydration interactions were not included because the corresponding parameters were unavailable. Thus,

$$V_{\mathrm{EDLVO}} = V_{\mathrm{vdW}} + V_{\mathrm{EDL}} + V_{\mathrm{HA}} \tag{3}$$

where V_{HA} is the hydrophobic interaction energy.

All calculations were performed in aqueous media at pH 8.0 and 298.15 K in the presence of 1.0×10^{-3} mol/L KCl. The ionic strength was calculated as follows:

$$I = \frac{1}{2}\sum\nolimits_i c_i z_i^2 \tag{4}$$

where I is the ionic strength, c_i is the molar concentration of ion i, and z_i is its valence. For the 1×10^{-3} mol/L KCl solution, $I = 1.0 \times 10^{-3}$ mol/L. The particles were assumed to be identical spheres with a diameter of 74 μm, corresponding to $R_1 = R_2 = R = 37$ μm.

DLVO/EDLVO calculations were performed for two identical spherical particles in water at pH 8.0 and 298.15 K in the presence of 1.0×10^{-3} mol/L KCl. The zeta-potential values measured under the corresponding reagent conditions were used as input parameters for the calculations. The particle diameter and radius were set to 74 μm and 37 μm, respectively. The relative permittivity of water was taken as $\varepsilon_r = 78.54$ at 298.15 K, and the vacuum permittivity was set to $\varepsilon_0 = 8.854 \times 10^{-12}$ F/m [29]. All distances were converted to metres before calculation.

The van der Waals interaction energy was calculated as follows:

$$V_{\mathrm{vdW}} = -\frac{A_{132}R}{12\mathrm{h}} \tag{5}$$

where A_{132} is the effective Hamaker constant. For cassiterite, $A_{11} = 25.6 \times 10^{-20}$ and $A_{33} = 4.38 \times 10^{-20}$ J, giving $A_{132} = \left(\sqrt{A_{11}} - \sqrt{A_{33}}\right)^2$ [30].

The electrostatic double-layer interaction energy was calculated using:

$$V_{\mathrm{EDL}} = 2\pi\varepsilon_0\varepsilon_r R\zeta^2 \ln[1 + exp(-\kappa \mathrm{h})] \tag{6}$$

where ζ is the zeta potential obtained from Figure 14 and κ^{-1} is the Debye length.

The Debye screening parameter was calculated from the ionic strength of the suspension according to:

$$\kappa = \left(\frac{2e^2 N_A I}{\varepsilon_0\varepsilon_r k_B T}\right)^{1/2} \tag{7}$$

where N_A is Avogadro's constant, k_B is the Boltzmann constant, and T is the absolute temperature.

For bornite, the hydrophobic interaction energy was calculated as follows:

$$V_{HA} = -\frac{K_{132}R}{12h} \quad (8)$$

where K_{132} is the effective hydrophobic interaction constant, analogous to the Hamaker constant used for van der Waals interactions.

$$K_{132} = \sqrt{K_{131}K_{232}} \quad (9)$$

where K_{131} and K_{232} are the hydrophobic interaction constants for the corresponding particle–water interfaces. It was estimated from the water contact angle according to:

$$\log K_{132} = a \times \cos\theta + b \quad (10)$$

where θ is the water contact angle, $a = -3.2$ and $b = -18.229$ [31].

The interaction force was consistently defined as $F(h) = -dV/dh$; therefore, negative and positive values represent attraction and repulsion, respectively. All distances were expressed in metres in the calculations.

3. Results and Discussion

3.1. Grinding Results

For the polymetallic ore, the main valuable minerals are cassiterite and copper sulfide minerals. Cassiterite is often recovered by gravity separation due to its high density, and the suitable feed particle size range is 0.019–2 mm. Sulfide minerals are often recovered by flotation, and the suitable feed particle size range is 0.038–0.15 mm [32]. Therefore, in this study, the −0.15 + 0.019 mm fraction in the grinding products was selected as the target size fraction, whereas the −0.019 mm fraction was regarded as the overground fraction.

Lime is commonly employed in the grinding process at the Datun plant as both a pH regulator and an inhibitor, with the aim of controlling the pulp environment, suppressing the excessive activation of certain gangue minerals, and thereby improving the selectivity of subsequent flotation. Figure 3 compares the particle-size distributions of the grinding products obtained with and without the addition of 0.1 wt% lime. As shown in Figure 3, the addition of lime affected the particle-size composition of the grinding products. Specifically, the yield of the coarse fraction (+0.15 mm) decreased markedly, indicating that large particles were more effectively broken down and that mineral liberation was enhanced in the presence of lime. Meanwhile, the proportion of the target size fraction (−0.15 + 0.019 mm) increased, suggesting that an appropriate amount of lime promotes the generation of target-size particles and provides a more favorable particle-size basis for downstream beneficiation. In contrast, the effect of lime on the overground fraction (−0.019 mm) was relatively minor, implying that its primary role was to reduce the retention of coarse particles and enhance the production of suitable size fractions without substantially increasing overgrinding. These results demonstrate that, in addition to its conventional functions of pH regulation and gangue-mineral depression, lime promotes particle breakage under the tested grinding conditions, resulting in a decrease in the coarse fraction and an increase in the target size fraction.

Previous studies have demonstrated that STPP exhibits a remarkable grinding aid effect in pure mineral systems, primarily by adsorbing onto mineral surfaces to alter their physicochemical properties, thereby reducing particle agglomeration and improving wettability [12]. Building on this understanding, the present study introduced STPP into the grinding process of a copper–tin polymetallic sulfide ore to evaluate its influence on particle size distribution and grinding efficiency. Figure 4 illustrates the particle size composition of grinding products under different STPP dosages. As the STPP concentration increased,

the particle-size distribution changed systematically. Specifically, the proportion of the coarse fraction (+0.15 mm) decreased, indicating that STPP promoted the breakage of large particles and accelerated mineral liberation. Meanwhile, the proportion of the target size fraction (−0.15 + 0.019 mm) increased by 2.04%, indicating that STPP promoted the formation of the target fraction and improved grinding selectivity. Although a slight increase in the overground fraction (−0.019 mm) was observed, the change was relatively small, suggesting that an appropriate STPP dosage did not cause significant overgrinding. When the STPP dosage exceeded 0.05 wt%, the coarse fraction increased, whereas the target fraction decreased, indicating that excessive STPP addition was unfavorable for obtaining the desired grinding product.

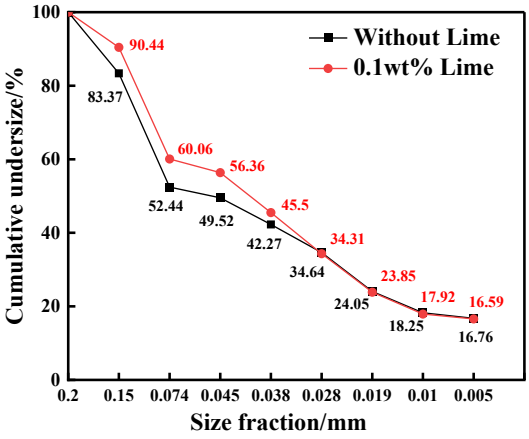


Figure 3. Particle-size distribution of ground ore with and without lime addition.

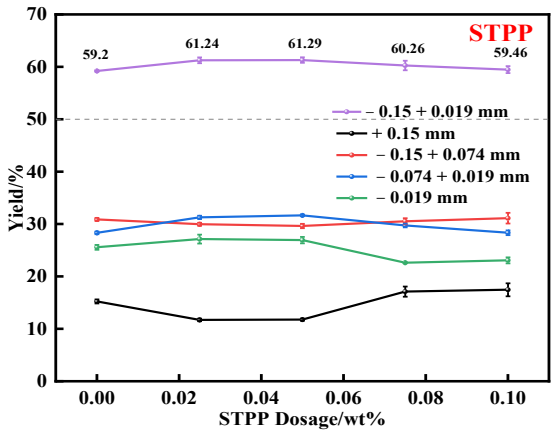


Figure 4. Effect of STPP dosage on the particle-size distribution of grinding products.

Based on the preceding results, the effect of STPP addition on the grinding performance of the copper–tin polymetallic sulfide ore in the presence of lime was further investigated. The experimental results are presented in Figure 5. Compared with lime addition alone, the addition of 0.025 wt% STPP further increased the proportion of the target size fraction, while the fine-particle content remained nearly unchanged and the coarse fraction decreased. These results indicate that an appropriate STPP dosage promoted the transformation of coarse particles into the target fraction while limiting overgrinding. When the STPP dosage was increased to 0.05 wt%, the improvement in the target fraction was reduced, suggesting that excessive STPP addition was unfavorable for optimizing the grinding-product characteristics.

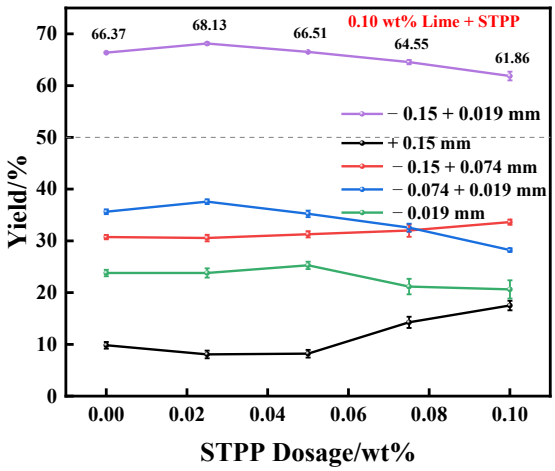


Figure 5. Particle-size distribution of ground ore under the action of lime and different amounts of STPP.

A comparative analysis of Figures 4 and 5 shows that the addition of STPP (0.025 wt%) in the presence of lime (0.10 wt%) improved the grinding performance of the copper–tin polymetallic sulfide ore. Compared with grinding without reagents, the proportion of the target fraction increased from 59.20% to 68.13%, representing an increase of 8.93 percentage points. Compared with the lime-only condition, the proportion of the intermediate, readily separable size fraction increased from 66.37% to 68.13%, corresponding to an increase of 1.76 percentage points. These results indicate that the addition of STPP improved the particle-size distribution of the grinding products by increasing the proportion of target-sized particles while causing little change in the overground fraction.

3.2. Copper–Tin Separation Tests

3.2.1. Effect of STPP Addition on Copper Flotation Performance

STPP is commonly used as a depressant in flotation processes [33,34]. During grinding, the breakage of bornite may expose fresh mineral surfaces and potentially facilitate the release of copper species into the slurry. Previous studies have reported that STPP exhibits strong chelating ability [35] and can form stable complexes with Cu(II) ions in solution under near-neutral conditions [34]. Based on these findings, STPP may complex with dissolved Cu(II) ions, potentially reducing the concentration of free Cu(II) in the slurry and affecting interactions between copper ions and collectors. However, copper species release and complexation by STPP were not directly investigated in this study; therefore, this mechanism should be regarded as a possible explanation.

The grinding tests indicated that the addition of 0.025 and 0.05 wt% STPP in combination with lime reduced the coarse fraction and increased the proportion of the target size fraction. Figure 6 shows the effects of adding STPP at dosages of 0, 0.025, and 0.05 wt% during grinding on copper flotation performance.

As shown in Figure 6, the addition of 0.025 wt% STPP resulted in the highest copper concentrate grade and copper recovery among the tested conditions, reaching 2.89% and 71.79%, respectively. When the STPP dosage was increased to 0.05 wt%, both the copper concentrate grade and copper recovery decreased. These results demonstrate that copper flotation performance varied with STPP dosage, with 0.025 wt% STPP resulting in a higher concentrate grade and recovery than 0.05 wt% STPP under the tested conditions. Therefore, considering both the grinding and flotation results, 0.025 wt% STPP was selected for subsequent experiments.

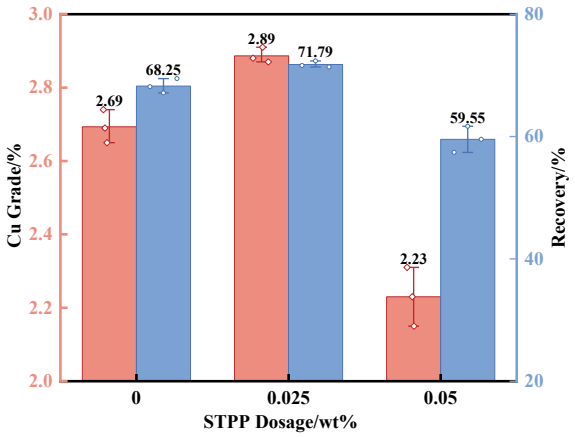


Figure 6. Effect of STPP dosage on copper flotation.

Previous studies suggest that the improvement in flotation performance at a relatively low STPP dosage may be associated with its dispersing effect on fine particles, its potential interactions with Ca- and Mg-containing gangue minerals, and its possible complexation with dissolved metal ions [12,34–36]. These effects may alter the physicochemical conditions of the pulp and consequently influence bubble–particle attachment. At a higher STPP dosage, changes in mineral surface properties or interference with collector adsorption may contribute to the observed decrease in flotation performance. However, these mechanisms were not directly verified in the present study and should therefore be regarded as possible explanations. This interpretation is consistent with previous studies reporting adverse effects of excessive STPP addition under certain flotation conditions [37].

3.2.2. Effect of STPP Addition on Cassiterite Separation Performance

Coarse-grained cassiterite is typically recovered by gravity separation, whereas fine-grained cassiterite requires flotation [38,39]. The effects of STPP addition on the separation of coarse-grained cassiterite by shaking-table separation and on the flotation of fine-grained cassiterite were investigated, and the results are shown in Figure 7. As shown in Figure 7a, increasing the STPP dosage improved both the grade and recovery of the tin concentrate obtained by gravity separation. At an STPP dosage of 0.025 wt%, the tin grade and recovery increased by 0.44% and 14.31%, respectively, compared with the condition without STPP. This improvement may be related to the dispersing effect of STPP, which enhances the dispersion of mineral particles in the pulp and facilitates the separation of cassiterite from gangue minerals during gravity separation [12,23]. In contrast, Figure 7b shows that STPP addition decreased both the grade and recovery of cassiterite in the subsequent flotation stage. STPP has been reported to affect mineral-surface wettability and exhibit depressant effects in flotation systems, which may reduce the floatability of cassiterite under certain conditions [37–40]. Therefore, the opposite responses observed in the two separation stages may be associated with the different effects of STPP on particle dispersion during gravity separation and on mineral-surface properties during flotation.

It should be noted that most of the cassiterite was recovered during the gravity separation stage, whereas the contribution of the subsequent flotation stage to the overall Sn recovery was relatively limited. To evaluate the effect of STPP on the complete separation process, the overall Sn recovery obtained by combining the gravity separation and subsequent flotation stages was further calculated. At STPP dosages of 0, 0.025, and 0.05 wt%, the overall Sn recoveries were 92.58%, 93.56%, and 92.39%, respectively. Compared with the condition without STPP, the addition of 0.025 wt% STPP increased the overall Sn recovery by 0.98%, despite the decrease in cassiterite flotation performance. This indicates that the

improvement in the gravity separation stage largely compensated for the adverse effect of STPP on subsequent flotation. However, further increasing the STPP dosage to 0.05 wt% resulted in a decrease in overall Sn recovery to 92.39%, indicating that the deterioration in flotation performance outweighed the additional benefit obtained during gravity separation. Therefore, the effect of STPP on cassiterite separation should be evaluated based on the combined performance of gravity separation and flotation rather than the results of either separation stage alone.

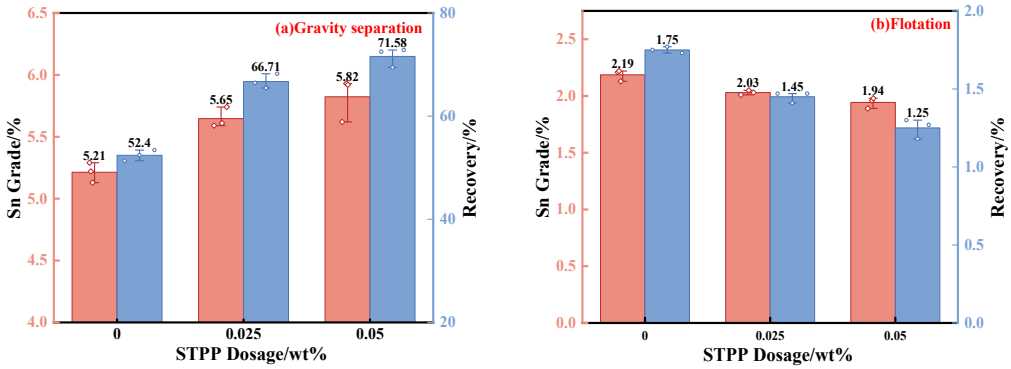


Figure 7. Effect of STPP on cassiterite recovery: (**a**) gravity concentration and (**b**) flotation.

Based on a comprehensive analysis of the grinding test results and subsequent copper–tin separation experiments, 0.025 wt% STPP was selected for subsequent experiments. At this dosage, STPP modified the particle-size distribution by increasing the proportion of intermediate-sized particles while reducing the coarse and overground fractions, thereby providing a more favorable particle-size distribution for subsequent separation processes.

3.3. Particle-Size Distribution and Mineral Liberation Characteristics

The MapsMin automated mineral analysis system is widely used in mineral processing to characterize particle size, mineralogy, and process performance. In this study, it was used to assess the effects of STPP on mineral liberation, particle-size distribution, and particle morphology. The grinding products obtained with lime and 0 or 0.025 wt% STPP were compared, with particular emphasis on the liberation and particle-size characteristics of the major minerals.

3.3.1. Particle Size Distribution of the Ore

Figure 8a presents the particle-size distribution curves of the grinding products obtained with lime (0.1 wt%) alone and with the combined addition of lime and STPP (0.1 wt% + 0.025 wt%), whereas Figure 8b shows the corresponding particle morphologies. The characteristic particle-size parameters (D_{10}, D_{50}, and D_{90}) obtained from MapsMin analysis are summarized in Table 3. Figure 9 presents the particle-size distributions of bornite and cassiterite, and the corresponding D_{10}, D_{50}, and D_{90} values are summarized in Table 4. As shown in Figure 8a, the addition of STPP significantly altered the particle-size distribution of the grinding products. The maximum particle size, expressed as the equivalent perimeter diameter, decreased from 820.95 to 495.30 μm. This trend is further supported by the characteristic particle-size parameters listed in Table 3. Compared with the lime-only condition, the addition of STPP decreased the D_{10}, D_{50}, and D_{90} values from 49, 176, and 374 μm to 30, 108, and 237 μm, respectively. These results demonstrate an overall refinement of the grinding products and a substantial reduction in the coarse-particle fraction. The full particle-size distribution curve also shows that the proportion of coarse particles decreased markedly after STPP addition, whereas the proportion of intermediate-sized particles in-

creased, resulting in a narrower and more concentrated distribution. In the intermediate size range of 60–470 μm, the curve obtained with STPP remained below that obtained with lime alone. This indicates that, at a given cumulative yield, the particle sizes were more concentrated within the intermediate range after STPP addition. Alternatively, for a given particle-size interval, STPP increased the yield of this fraction. Meanwhile, the fine-particle fraction did not increase substantially, suggesting that STPP promoted the breakage of coarse particles without causing severe overgrinding. The morphological observations in Figure 8b are consistent with the particle-size results. After STPP addition, the grinding products exhibited a finer and more uniformly distributed particle morphology, with fewer coarse particles and less pronounced particle aggregation.

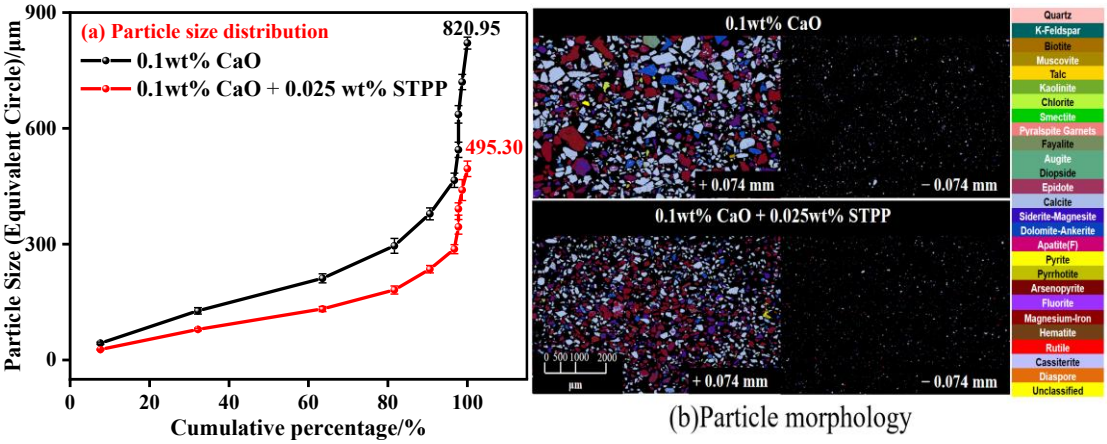


Figure 8. Particle size distribution (**a**) and particle morphology (**b**) of the grinding products under different reagent conditions.

Table 3. Characteristic particle-size parameters (D10, D50, and D90) of the copper–tin polymetallic sulfide ore under different reagent conditions, based on MapsMin analysis.

Reagent Condition	D_{10}/μm	D_{50}/μm	D_{90}/μm
0.10 wt% CaO	49	176	374
0.10 wt% CaO + 0.025 wt% STPP	30	108	237

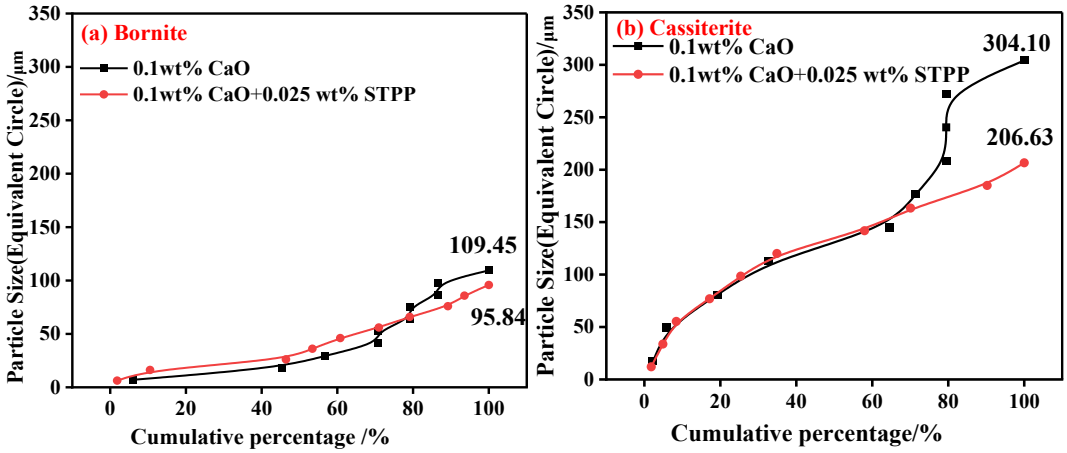


Figure 9. Particle-size distribution of bornite (**a**) and cassiterite (**b**) in the copper–tin polymetallic sulfide ore.

Table 4. D10, D50, and D90 values of bornite and cassiterite under different reagent conditions, determined by MapsMin analysis.

Reagent Condition	Bornite			Cassiterite		
	D_{10}/μm	D_{50}/μm	D_{90}/μm	D_{10}/μm	D_{50}/μm	D_{90}/μm
0.10 wt% CaO	8	23	100	58	130	288
0.10 wt% CaO + 0.025 wt% STPP	13	34	80	58	134	186

As shown in Figure 9, the maximum particle size of bornite decreased from 109.45 to 95.84 μm, whereas that of cassiterite decreased from 304.10 to 206.63 μm after STPP addition. The corresponding characteristic parameters in Table 4 provide further details. For bornite, the D_{90} value decreased from 100 to 80 μm, whereas the D_{10} and D_{50} values increased from 8 and 23 μm to 13 and 34 μm, respectively. For cassiterite, the D_{90} value decreased markedly from 288 to 186 μm, the D_{10} value remained unchanged at 58 μm, and the D_{50} value increased slightly from 130 to 134 μm. The decrease in D_{90} for both minerals indicates effective fragmentation of the coarse-particle fraction, whereas the slight increases in D_{50} for bornite and cassiterite reflect the redistribution of particles from the coarse fraction toward the intermediate-size range rather than excessive generation of fines. Overall, these results demonstrate that STPP promotes the effective breakage of coarse particles and produces a more suitable particle-size distribution for subsequent beneficiation.

3.3.2. Mineral Liberation of the Ore

Mineral liberation refers to the percentage of liberated mineral particles (by number or mass) relative to the total number (or mass) of particles of the target mineral. It is an important indicator for evaluating the degree of mineral liberation and directly influences the efficiency of subsequent flotation processes. Figure 10 presents a comparison of the liberation degrees of the major minerals in the copper–tin polymetallic sulfide ore with and without STPP addition. Figure 11 illustrates the association relationships of bornite and cassiterite, including free surface (FS), binary-phase association (BP), ternary-phase association (TP), and complex association (CA).

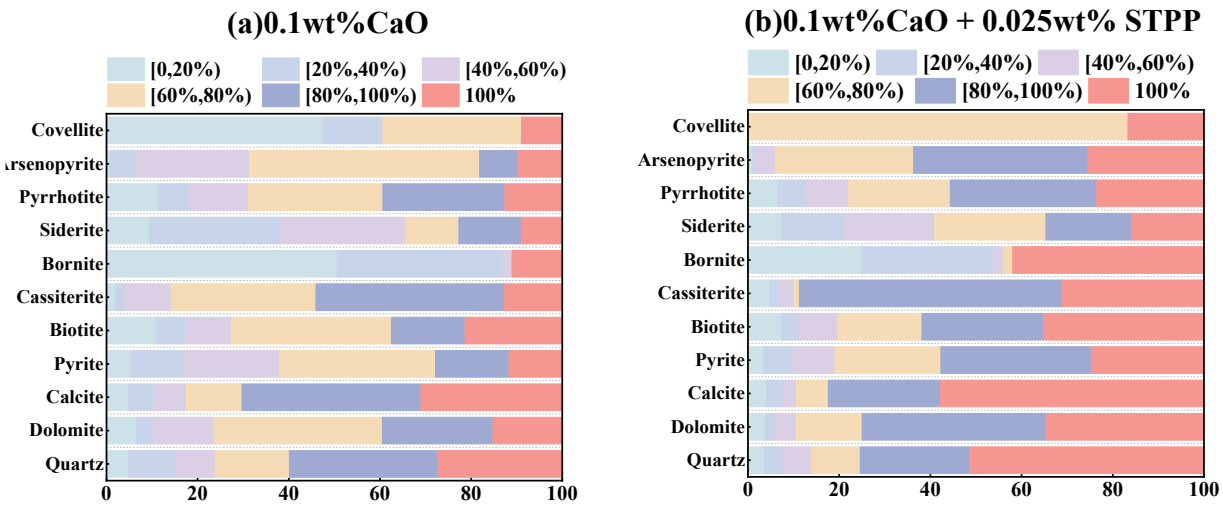


Figure 10. Liberation classes of the major minerals in the grinding products without STPP and with 0.025 wt% STPP.

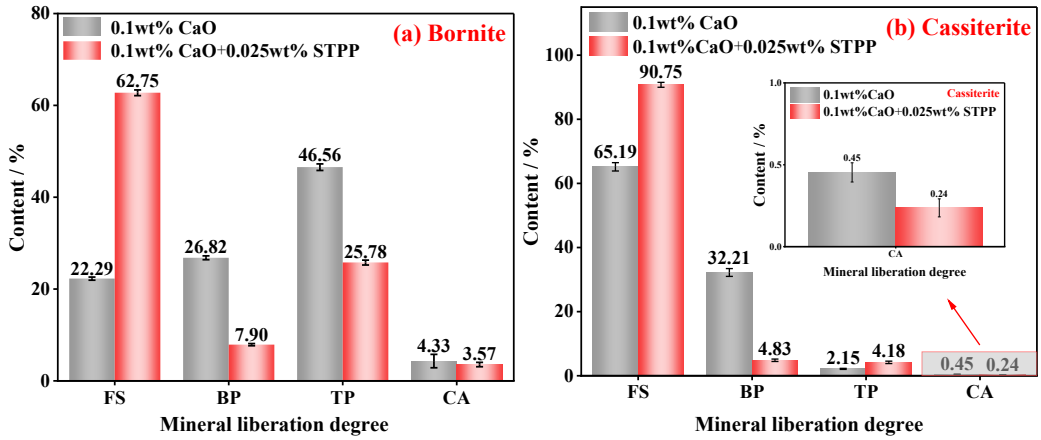


Figure 11. Association relationships of bornite (**a**) and cassiterite (**b**), including free surface (FS), binary-phase association (BP), ternary-phase association (TP), and complex association (CA).

As shown in Figure 10, the degree of complete liberation of valuable minerals such as cassiterite and bornite increased significantly after the addition of STPP. Specifically, the complete liberation degrees of both cassiterite and bornite increased with the addition of STPP. Meanwhile, other major minerals such as quartz, calcite, and dolomite also exhibited varying degrees of improvement in liberation. These results indicate that STPP can effectively promote the breakage and liberation of mineral particles during the grinding process, thereby increasing the proportion of liberated valuable minerals in the grinding products.

Further analysis based on Figure 11 shows that the proportion of FS for both cassiterite and bornite particles increased after the addition of STPP compared with the system without STPP. This suggests that the addition of STPP reduces the proportion of composite particles between minerals, allowing valuable minerals to exist more frequently as liberated grains. This phenomenon may be attributed to the adsorption of STPP on mineral surfaces during the grinding process, which enhances electrostatic repulsion between particles and reduces particle agglomeration, thereby promoting particle dispersion and mineral liberation [12].

The improvement in mineral liberation provides more favorable particle conditions for subsequent separation processes. On the one hand, a higher proportion of liberated particles increases the probability of effective interaction between collectors and valuable minerals. On the other hand, the reduction in composite particles improves the selectivity of mineral separation. Consequently, during subsequent flotation or gravity separation processes, collectors can interact more effectively with valuable mineral particles, ultimately improving the grade and recovery of the concentrates.

3.4. Surface Morphological and Elemental Characteristics

To further characterize the morphological characteristics of the grinding products, scanning electron microscopy (SEM) was employed to compare the particle surfaces obtained under different reagent conditions, as shown in Figure 12.

As shown in Figure 12a, the particles ground without STPP exhibit a relatively heterogeneous morphology, with numerous elongated particles, sharp cassiterite fracture surfaces, and a few surface pores. In contrast, Figure 12b shows a more uniform particle morphology after STPP addition. The cassiterite surfaces exhibit irregular and stepped fracture planes, while more surface agglomerates were observed in the STPP-treated sample. Similar changes in surface morphology and the development of surface defects after STPP addition have been reported during the wet grinding of mineral particles [12,32]. These differences may be associated with the interaction of STPP with mineral surfaces during grinding, which can modify surface properties and particle–particle interactions [12]. The

irregular and stepped fracture features may reflect differences in the development of fracture surfaces, whereas the observed surface agglomerates may be related to the retention or aggregation of fine particles on mineral surfaces.

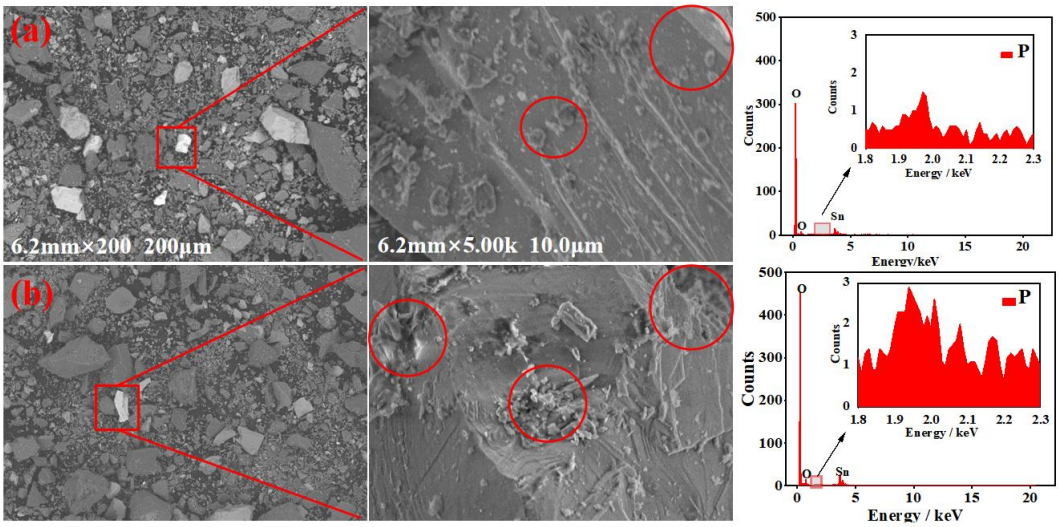


Figure 12. SEM and EDS characterization of cassiterite in mill products. (**a**) 0.10 wt% CaO; (**b**) 0.10 wt% CaO + 0.025 wt% STPP.

3.5. Surface Wettability Characteristics

Once grinding aid reagents are adsorbed onto mineral surfaces, they can significantly modify surface properties, particularly wettability, which plays a crucial role in subsequent separation processes such as flotation [12]. According to the mineralogical data presented in Table 2, the primary valuable minerals in the studied ore are cassiterite and bornite. Therefore, the effects of STPP addition on the surface wettability of cassiterite and bornite were investigated by contact-angle measurements; the molecular structure of STPP is also shown in Figure 13.

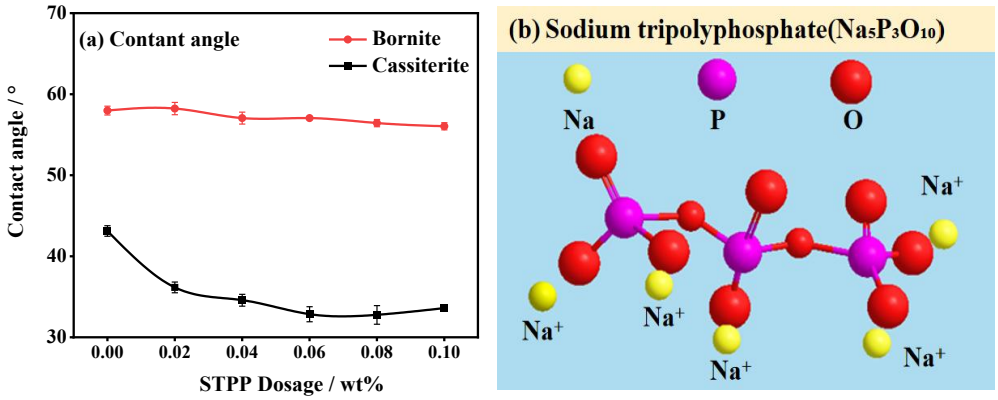


Figure 13. (**a**) Effect of STPP dosage on the contact angles of cassiterite and bornite; (**b**) molecular structure of sodium tripolyphosphate (STPP).

The experimental results demonstrate that the contact angle of cassiterite decreases markedly upon the addition of STPP, indicating an increase in surface hydrophilicity. This change suggests that STPP adsorption may modify the surface properties of cassiterite and enhance its affinity for water. As the concentration of STPP increases, the contact angle changes more gradually and eventually stabilizes, suggesting that the effect of STPP on

cassiterite wettability tends to level off [41]. Although no collector was used in the contact-angle experiments, the increased hydrophilicity of cassiterite may be unfavorable for its subsequent flotation [42,43].

In contrast, the contact angle of bornite showed only minor variations after STPP addition and remained within the experimental margin of error [12]. This suggests that STPP had a limited effect on the macroscopic wettability of the bornite surface under the tested conditions.

Overall, these findings indicate that STPP affects the wettability of cassiterite and bornite differently, suggesting its potential role in regulating the surface properties of minerals and influencing subsequent flotation behavior. However, the relationship between STPP adsorption, collector interactions, and flotation performance requires further verification under actual flotation conditions.

3.6. Surface Charge Characteristics

Zeta potential is a key indicator of the surface charge of minerals, and its variation reflects the influence of additives on mineral surfaces [44]. Figure 14 shows the zeta potentials of cassiterite and bornite under different conditions. STPP altered the zeta potentials of both minerals, indicating changes in their surface-charge environments. This change may arise from interactions between STPP and surface copper sites or from modification in the electrical double layer [36,45]. These results indicate that STPP regulates the surface electrochemical properties of both cassiterite and bornite, thereby influencing their interactions with flotation reagents and their subsequent separation behavior.

The response of the two minerals differs because of their distinct surface chemical properties and interactions with STPP [46]. The relatively small change in the contact angle of bornite indicates that the modification in its surface charge was not accompanied by a pronounced change in macroscopic wettability. Thus, the effect of STPP on bornite is more clearly reflected in its surface-charge characteristics than in its contact angle. This interpretation distinguishes the adsorption-induced modification in the mineral surface from the net interaction between bornite particles.

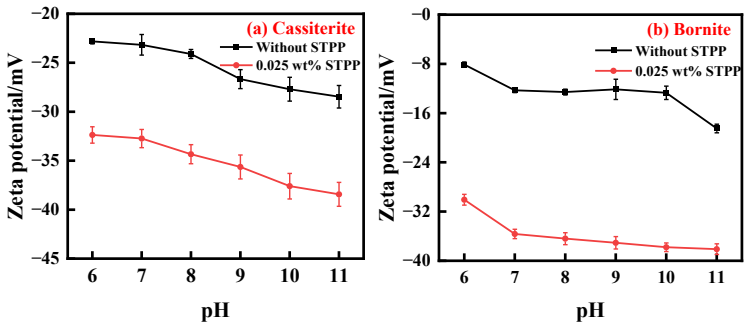


Figure 14. Zeta potentials of cassiterite (**a**) and bornite (**b**) as a function of pH with and without STPP addition.

3.7. Interaction Energy Estimation Using DLVO and Extended DLVO Theory

To further clarify the effect of STPP on the interparticle interactions of cassiterite and bornite, the DLVO/EDLVO interaction energies under different STPP conditions were calculated, and the corresponding results are shown in Figures 15 and 16.

Figure 15 shows the DLVO interaction energy between cassiterite particles as a function of surface separation distance. As shown in Figure 15, STPP addition increases the interaction energy barrier between cassiterite particles, indicating enhanced electrostatic repulsion and improved particle dispersion in the slurry. Considering the complex mineralogical

composition of the ore, STPP may interact with the surfaces of some gangue minerals, potentially contributing to pulp dispersion.

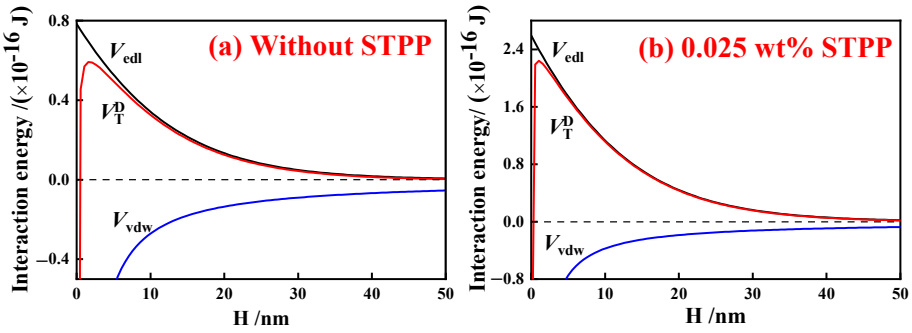


Figure 15. DLVO interaction energy between cassiterite particles as a function of surface separation distance under different reagent conditions. (**a**) Without STPP; (**b**) 0.025 wt% STPP.

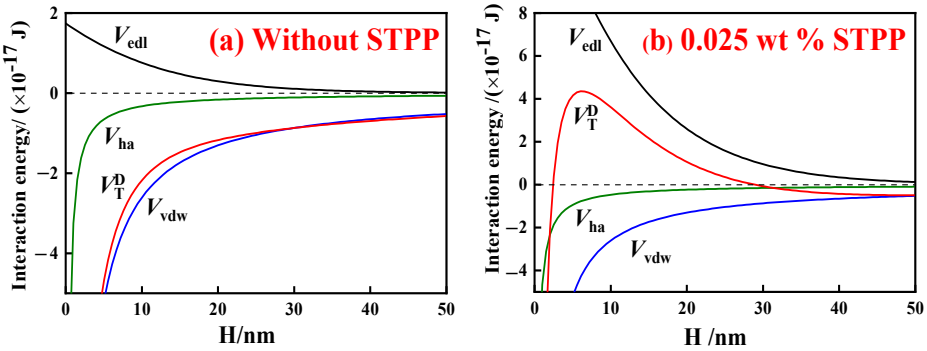


Figure 16. EDLVO interaction energy between bornite particles as a function of surface separation distance under different reagent conditions. (**a**) Without STPP; (**b**) 0.025 wt % STPP.

Figure 16 presents the EDLVO interaction energy between bornite particles as a function of surface separation distance. Similar to cassiterite, STPP addition increases the interaction energy barrier between bornite particles, indicating a reduced tendency toward aggregation and enhanced particle dispersion. This result describes the net particle–particle interaction and does not imply weak adsorption of STPP on the bornite surface; adsorption can modify the surface charge and wettability without increasing the net attractive interaction between particles.

Enhanced mineral-particle dispersion can improve grinding effectiveness by altering particle–particle interactions within the slurry. Increased repulsive interactions inhibit particle aggregation, allowing mineral particles to remain more uniformly dispersed and increasing their exposure to the grinding media. This favors effective collisions and energy transfer between the grinding media and mineral particles, thereby promoting the breakage of relatively coarse particles and reducing undergrinding.

Meanwhile, improved dispersion of fine particles reduces the formation of compact agglomerates during grinding. This limits the repeated breakage of fine particles within agglomerates and consequently alleviates overgrinding. The simultaneous promotion of coarse-particle breakage and suppression of excessive fine-particle breakage results in a more balanced grinding process, contributing to an increased proportion of intermediate-sized particles (−0.15 + 0.019 mm) and a more favorable particle-size distribution.

Overall, the DLVO/EDLVO results demonstrate that STPP enhances the dispersion of cassiterite and bornite particles by increasing the interparticle interaction energy barrier. The resulting improvement in particle dispersion promotes more effective grinding

and contributes to a more balanced particle-size distribution, which is beneficial for the subsequent flotation and gravity separation of copper and cassiterite.

4. Conclusions

This study systematically investigated the role and application potential of STPP as a grinding aid in the processing of a copper–tin polymetallic sulfide ore. The following conclusions were drawn:

The grinding results showed that, compared with the lime-only condition (0.10 wt% lime), the addition of 0.025 wt% STPP increased the proportion of the target size fraction (−0.15 + 0.019 mm) by 1.76%, without a marked increase in the fine fraction (−0.019 mm) or the coarse fraction (+0.15 mm). Compared with the lime-only condition, the addition of 0.025 wt% STPP increased the grade and recovery of the copper flotation concentrate by 0.20% and 3.54%, respectively, and those of the cassiterite gravity concentrate by 0.44% and 14.31%, respectively. The overall Sn recovery of the combined gravity separation and flotation process increased from 92.58% under the lime-only condition to 93.56% with the addition of 0.025 wt% STPP, but decreased to 92.39% when the STPP dosage was increased to 0.050 wt%. Automated mineralogical analysis showed that STPP addition increased the complete liberation degrees of cassiterite and bornite, while varying degrees of improvement were also observed for other major minerals. With the addition of 0.025 wt% STPP, the maximum particle size decreased from 820.95 to 495.30 μm, and D90 decreased from 374 to 237 μm relative to the lime-only condition. Surface characterization and DLVO/EDLVO analysis indicated that STPP altered mineral surface properties and interparticle interactions, which may have contributed to the observed changes in particle-size distribution and mineral liberation.

Author Contributions: X.L.: Data curation, Formal analysis, Investigation, Methodology, Visualization, Writing—original draft, Writing—review & editing. Q.X.: Resources, Supervision, Formal analysis, Investigation, Methodology, Visualization, Writing—review & editing. M.W.: Investigation, Methodology, Project administration, Validation, Writing—review & editing. C.Z.: Investigation, Methodology, Visualization, Writing—review & editing. Y.C.: Resources. S.J.: Resources, Supervision, Formal analysis, Investigation, Methodology, Visualization, Writing—review & editing. All authors have read and agreed to the published version of the manuscript.

Funding: This work is funded by the National Natural Science Foundation of China (Youth Science Fund Project, Category C; Grant No. 52504298) and Yunnan Fundamental Research Projects (grant No. 202401CF070154). The authors would like to express their gratitude to all members of the Yunnan Provincial University Selective Grinding Quality Improvement and Consumption Reduction Scientific and Technological Innovation Team.

Data Availability Statement: Data will be made available on request.

Conflicts of Interest: The authors declare that they have no known competing financial interests or personal relationships that could have appeared to influence the work reported in this paper.

References

1. Wang, G.B.; Xiao, Q.F.; Zhou, Q.; Liu, X.Y.; Jin, S.Z.; Jin, Y.J.; Shen, C.A. An innovatory approach for determining grinding media system to optimize fraction compositions of grinding products based on grinding dynamics principle. *Powder Technol*. **2024**, *434*, 119302. [CrossRef]
2. He, F.; Sun, C.Y.; Lei, S. Effects of grinding media on surface properties and flotation behaviour of galena. *Nonferrous Met*. **2006**, *58*, 81–85.
3. Xu, L.H.; Hu, Y.H.; Wu, H.Q.; Tian, J.; Liu, J.; Gao, Z.Y.; Wang, L. Surface crystal chemistry of spodumene with different size fractions and implications for flotation. *Sep. Purif. Technol*. **2016**, *169*, 33–42. [CrossRef]
4. Sadrai, S.; Meech, J.; Ghomshei, M.; Sassani, F.; Tromans, D. Influence of impact velocity on fragmentation and the energy efficiency of comminution. *Int. J. Impact Eng*. **2006**, *33*, 723–734. [CrossRef]

5. Radziszewski, P. Developing an experimental procedure for charge media wear prediction. *J. Miner. Eng.* **2000**, *13*, 949–961. [CrossRef]
6. Tian, D.L.; Yin, W.Z.; Xie, Y.; Liu, J.Y.; Zhu, Z.L.; Yao, J. Influence of surface roughness of magnesite on bubble-particle energy barrier: Analysis based on a new simplified model. *Colloids Surf. A Physicochem. Eng. Asp.* **2024**, *681*, 132860. [CrossRef]
7. Yuan, Y.Z.; Zhang, Y.M. Improvement of the grindability of vanadium-bearing shale and the direct vanadium leaching efficiency of grinded product via microwave pretreatment with particle size classification. *Colloids Surf. A Physicochem. Eng. Asp.* **2022**, *647*, 128979. [CrossRef]
8. Chipakwe, V.; Karlkvist, T.; Rosenkranz, J.; Chelgani, S.C. Exploring the effect of a polyacrylic acid-based grinding aid on magnetite-quartz flotation separation. *Sep. Purif. Technol.* **2023**, *305*, 12253. [CrossRef]
9. Fan, C.Y.; Ren, L.Y.; Zhang, Y.M.; Bao, S.X.; Yang, Z.L. Influence of sodium hexametaphosphate on muscovite grinding and its mechanism analysis. *Minerals* **2023**, *13*, 457. [CrossRef]
10. Xie, D.; Hou, Y.; Gai, Z.; Huang, G.; Qi, S.F.; Xu, D.L.; Han, C.; Chen, L.B.; Zhu, J.J. Influence of grinding aids on grinding kinetics of oxidized iron ore. *J. Cent. South Univ. Sci. Technol.* **2020**, *51*, 279–286.
11. Du, L.; Zhou, W.; Liu, J.; Li, D. Research progress of cement grinding aids. *Mater. Rev.* **2009**, *23*, 80–84.
12. Mao, Y.; Liu, W.G.; Chen, X.D.; Wang, Z.H.; Liu, W.B.; Sun, W.H.; Shen, Y.B. The role of sodium tripolyphosphate in wet grinding process of magnesite. *Colloids Surf. A Physicochem. Eng. Asp.* **2023**, *668*, 131449. [CrossRef]
13. Cheng, F.; Feng, Y.; Su, Q.Q.; Wei, D.D.; Wang, B.; Huang, Y.W. Practical strategy to produce ultrafine ceramic glaze: Introducing a polycarboxylate grinding aid to the grinding process. *Adv. Powder Technol.* **2019**, *30*, 1655–1663. [CrossRef]
14. Yang, R.H.; Zhang, P.Y.; Huang, T.Y.; Wang, D.M.; Sun, Q.; Li, Y.; Mao, Z.Y.; Wang, W.S.; Song, X.W. Carbon reduction method for cement: Preparation of a new grinding aid based on environmentally friendly high-belite clinker. *J. Mater. Civ. Eng.* **2025**, *37*, 04025084. [CrossRef]
15. Mao, Y.; Wang, Z.H.; Liu, W.G.; Tian, P.C. Effect of TIPA/TEA combined grinding aid on the behavior of quartz flotation in DDA system. *Powder Technol.* **2022**, *406*, 117570. [CrossRef]
16. Wang, Z.; Wang, H.; Li, G.; Yu, F.J. Effect of Z-164D solution on bauxite strength and its mechanism. *J. Northeast. Univ. Nat. Sci.* **2014**, *35*, 112–116.
17. Chipakwe, V.; Karlkvist, T.; Rosenkranz, J.; Chelgani, S.C. Beneficial effects of a polysaccharide-based grinding aid on magnetite flotation: A green approach. *Sci. Rep.* **2022**, *12*, 6502. Correction in *Sci. Rep.* **2023**, 13, 5590.. [CrossRef]
18. Narayanan, S.; Raghunathan, N.; Nayak, U.B.; Lahiri, A.K. Environmental effects on grinding. *Int. J. Miner. Process.* **1983**, *10*, 309–317. [CrossRef]
19. Chipakwe, V. A comparative study on the effect of chemical additives on dry grinding of magnetite ore. *S. Afr. J. Chem. Eng.* **2020**, *34*, 74–81. [CrossRef]
20. Mao, Y.; Liu, W.G.; Liu, W.B.; Shen, Y.B.; Zhao, Q. Exploring the behavior of an alcoholic amine grinding aid in grinding-flotation system: Separation of quartz from magnesite. *J. Mol. Liq.* **2024**, *411*, 125783. [CrossRef]
21. Yang, X.; Lai, H.; Wei, X.; Shen, P.L.; Wang, Y.; Li, M.Y.; Cai, J.P.; Liu, D.W. Adsorption mechanism of Na2S2O3 and FeSO4 as a combined depressant for galena in bornite-galena flotation separation. *Colloids Surf. A Physicochem. Eng. Asp.* **2025**, *706*, 135799. [CrossRef]
22. Liu, J.; Hao, J.M.; Dong, W.C.; Zeng, Y. Depression mechanism of environment-friendly depressant dithiocarbamate chitosan in flotation separation of Cu-Zn sulfide. *Colloids Surf. A Physicochem. Eng. Asp.* **2021**, *615*, 126290. [CrossRef]
23. Mu, Y.F.; Peng, Y.J. Selectively depress copper-activated pyrite in copper flotation at slightly alkaline pH. *Min. Metall. Explor.* **2021**, *38*, 751–762. [CrossRef]
24. Churaev, N.V. The DLVO theory in Russian colloid science. *Adv. Colloid Interface Sci.* **1999**, *83*, 19–32. [CrossRef]
25. Li, Q.; Liao, C.L.; Hou, J.; Wang, W.J.; Zhang, J.S. A mathematic model based on eDLVO and Lifshitz theory calculating interparticle interactions in coal water slurry. *Fuel* **2022**, *316*, 123271. [CrossRef]
26. Liu, P.; Zhu, Y.W. Interaction between fine diamond particles in electroless nickel solutions. *J. Dispers. Sci. Technol.* **2015**, *36*, 1170–1177. [CrossRef]
27. Derjaguin, B.V.; Landau, L.D. Theory of the stability of strongly charged lyophobic sols and of the adhesion of strongly charged particles in solutions of electrolytes. *Acta Phys. Chim. URSS* **1941**, *14*, 633–662.
28. Verwey, E.J.W.; Overbeek, J.T.G. *Theory of the Stability of Lyophobic Colloids*; Elsevier: Amsterdam, The Netherlands, 1948.
29. Israelachvili, J.N. *Intermolecular and Surface Forces*, 3rd ed.; Academic Press: Amsterdam, The Netherlands, 2011. [CrossRef]
30. Albijanic, B.; Ozdemir, O.; Nguyen, A.V.; Bradshaw, D. Study of the influence of the crystallographic orientation of cassiterite observed with colloidal probe atomic force microscopy and its implications for hydrophobization by an anionic flotation collector. *ACS Omega* **2021**, *6*, 5670–5681. [CrossRef]
31. Jin, S.; Shi, Q.; Ou, L. Hydrophobic Flocculation of Fine Cassiterite Using Alkyl Hydroxamic Acids with Different Carbon Chain Lengths as Collectors. *Molecules* **2023**, *28*, 3911. [CrossRef]

32. Ma, S.; Li, H.; Shuai, Z.; Yang, J.; Deng, X.; Xu, W. Research on grinding law and grinding parameters optimization of polymetallic complex ores. *Minerals* **2022**, *12*, 1283. [CrossRef]
33. Mu, Y.F.; Peng, Y.J. The role of sodium metabisulphite in depressing pyrite in chalcopyrite flotation using saline water. *Miner. Eng*. **2019**, *142*, 105921. [CrossRef]
34. Cheng, L.L.; Chen, Y.X.; Liu, T.; Brouwers, H.J.H.; Yu, Q.L. Understanding the $CaCO_3$ phase transition of carbonated wollastonite composites caused by sodium tripolyphosphate: From amorphous to crystalline. *Cem. Concr. Compos*. **2024**, *148*, 105477. [CrossRef]
35. Houot, R.; Duhamet, D. The use of sodium-sulfite to improve the flotation selectivity between chalcopyrite and galena in a complex sulfide ore. *Miner. Eng*. **1992**, *5*, 343–355. [CrossRef]
36. Wang, Z.H.; Tian, P.C.; Mao, Y. Effects of grinding aids glycerol and sodium pyrophosphate on kinetic parameters of quartz grinding. *J. Northeast. Univ. Nat. Sci*. **2023**, *44*, 1009–1018.
37. Yao, J.; Yang, B.; Chen, K.Q.; Sun, H.R.; Zhu, Z.L.; Yin, W.Z.; Song, N.B.; Sheng, Q.Y. Sodium tripolyphosphate as a selective depressant for separating magnesite from dolomite and its depression mechanism. *Powder Technol*. **2021**, *382*, 244–253. [CrossRef]
38. Liu, S.Q.; Zhang, M.; Wang, W.P.; Song, B.X. A review on reagents and processes of fine-grained cassiterite flotation in mining engineering. *Adv. Mater. Res*. **2012**, *577*, 151–154. [CrossRef]
39. Zhao, J.H.; Wang, D.M.; Wang, X.G.; Liao, S.C.; Lin, H. Ultrafine grinding of fly ash with grinding aids: Impact on particle characteristics of ultrafine fly ash and properties of blended cement containing ultrafine fly ash. *Constr. Build. Mater.* **2015**, *78*, 250–259. [CrossRef]
40. Wang, X.; Jia, W.; Yang, C.; He, R.; Jiao, F.; Qin, W.; Cui, Y.; Zhang, Z.; Li, W.; Song, H. Innovative application of sodium tripolyphosphate for the flotation separation of scheelite from calcite. *Miner. Eng*. **2021**, *170*, 106981. [CrossRef]
41. Peng, Z.; Sun, L.; Cao, Y.; Fan, X.; Sun, W.; Wang, Q. Sodium Lauroyl Glutamate as a Collector in Cassiterite Flotation. *Minerals* **2023**, *13*, 61. [CrossRef]
42. Chau, T.T.; Bruckard, W.J.; Koh, P.T.L.; Nguyen, A.V. A review of factors that affect contact angle and implications for flotation practice. *Adv. Colloid Interface Sci*. **2009**, *150*, 106–115. [CrossRef]
43. Chen, Y.; Tong, X.; Feng, D.; Xie, X. Effect of Al (III) Ions on the Separation of Cassiterite and Clinochlore Through Reverse Flotation. *Minerals* **2018**, *8*, 347. [CrossRef]
44. Huang, S.; Huang, L.Y.; Li, Q.L.; Zhou, J.H.; Xu, Y.H.; Lv, J.F.; Xie, X. Study on the synergistic effect of sodium oleate/salicylaldoxime mixed collector co-adsorption on cassiterite flotation. *Adv. Powder Technol*. **2024**, *35*, 104634. [CrossRef]
45. Qian, Y.L.; Zhou, M.Y.; Zhang, Y.D.; Safarov, S.; Wang, Z. Comparative study on the effect of pyrophosphate and tripolyphosphate on the flotation separation of arsenopyrite and muscovite. *Minerals* **2024**, *14*, 785. [CrossRef]
46. Tafirenyika, T.P.; O'Connor, C.T.; Corin, K.C. Investigating the Influence of the Electrochemical Environment on the Flotation of Bornite and Chalcocite. *Minerals* **2022**, *12*, 1527. [CrossRef]

Disclaimer/Publisher's Note: The statements, opinions and data contained in all publications are solely those of the individual author(s) and contributor(s) and not of MDPI and/or the editor(s). MDPI and/or the editor(s) disclaim responsibility for any injury to people or property resulting from any ideas, methods, instructions or products referred to in the content.